



Coherent diffraction imaging of colloidal crystal grain in the divergent beam

Group: X-ray Crystallography

Illya Grygoryev, Karlsruhe Institute of Technology, Germany



Supervisors: Prof. Dr. Ivan Vartanians, Anatoly Shabalin,

Ruslan Kurta, Dmitry Dzhigaev

23 September, 2014

Abstract

In this report, the details of the lens-less microscopy approach are described. A test geometrical entity (icosahedron) has been built and filled by polystyrene spheres. Further, using the calculated intensity distribution and given field of the phase wave front, the internal structure of the object has been retrieved. The elaborated algorithms might be incorporated in the future Free Electron Laser applications and organic matter.

Contents

1. Introduction.....	4
2. Theoretical background	5
3. Experimental problem	8
4. Simulation of the experiment	9
6. Properties of the sample in the CXDI experiment.....	11
7. Results	12
8. Conclusion	15
9. Outlook.....	16
10. Acknowledgments	16
11. References.....	16

1. Introduction

Colloidal crystals have potential applications as *functional materials* (figure 1). They play significant role in the *optical computing*, as they can be formed into any shape to attain certain reflectance properties. Where *optical computing* is a research area that focuses on the development of the optical computer components, which would process binary data faster than the current based ones. Furthermore, *colloidal crystals* are used in the elaboration of the *future solar cells* (figure 3).

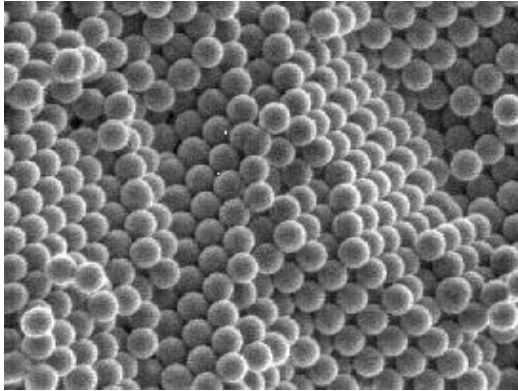


Figure 1: Self-organized colloidal crystals



Figure 2: Solar cells

In order to research the properties of the crystal it is necessary to understand its inner structure. X-ray crystallography utilizes diffraction theory for the reconstruction and analysis of the atomic grid of the crystal. Internal structure of the crystal can be identified by the *distribution of the electron density* in the crystal. The high quality in the reconstruction of the crystals *electron density distribution* is one of the main objectives in the Photon Science X-Ray Crystallography group at DESY (German Electron Synchrotron).

To test the reconstruction methods performing with the measurements from the divergent beam, the real experiment was simulated and the methods were applied to the simulated data.

In the chapter 2 *theoretical background* is discussed. The *experimental problem* is stated in chapter 3. The *simulation of the experiment* is explained in chapter 4. *Experiment setup* and *properties of the CXDI (Coherent X-Ray Diffraction Imaging)* are presented in chapters 5 and 6, respectively. Results are discussed in chapter 7. Chapters 8, 9 and 10 are dedicated to *Conclusion*, *Outlook* and *Acknowledgments*. *References* are given in chapter 11.

2. Theoretical background

In this work we investigated the interaction of the synchrotron radiation with a *Finite Size Crystal*. Synchrotron radiation is an electromagnetic radiation, with a wave length below 0.2 - 0.1 nm, emitted by electrons, oscillating in the periodic electromagnetic field. Modern synchrotron radiation sources can provide coherent and intense x-ray beam. Such sources have application in the number of imaging techniques. While investigating the interaction of the crystal with x-rays, we are interested in the electron density distribution of the sample in the real space:

$$\rho(\vec{r})$$

(1)

The *Fourier transform* of the electron density distribution (1) gives the complex scattered amplitudes in three dimensional reciprocal space of the sample:

$$A(\vec{q}) = \int \rho(\vec{r}) e^{-i\vec{q}\vec{r}} d\vec{r},$$

(2)

where \vec{q} is the momentum transfer vector:

$$\vec{q} = \vec{k}_f - \vec{k}_i,$$

(3)

where \vec{k}_f is the scattered wave vector and \vec{k}_i is the incident wave vector. Figure 1 depicts the scattering process and the intensities on the detector can be expressed as follows:

$$I(q_x, q_y) = |A(q_x, q_y)|^2,$$

(4)

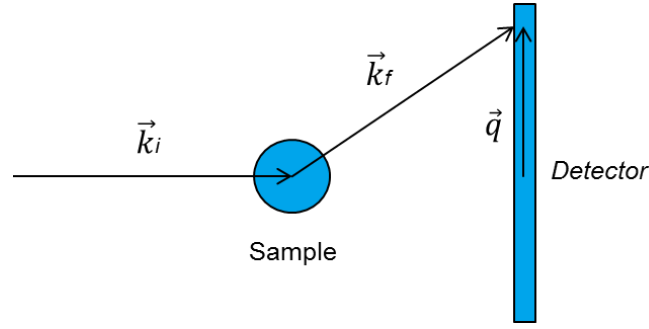


Figure 3: momentum transfer vector

The next step is to define the two dimensional complex function of the wave in the far-field in the reciprocal space:

$$w(q_x, q_y) = |A(q_x, q_y)|e^{-i*\varphi(q_x, q_y)}, \quad (5)$$

where $|A(q_x, q_y)|$ are the amplitudes in the two dimensional space, retrieved from the measured intensities (4) and $\varphi(q_x, q_y)$ are the corresponding phases. In the real experiment $\varphi(q_x, q_y)$ are obtained by means of the *phase retrieval algorithm* and during the simulation of the experiment they are provided by the simulation software.

The *Fourier transform* of $w(q_x, q_y)$ (5) is the two dimensional **projection of the electron density** in the beam direction in the real space:

$$p(x, y) = \mathcal{F}_{2D} \left(|A(q_x, q_y)|e^{-i*\varphi(q_x, q_y)} \right) \quad (6)$$

After measuring the sample from all perspectives (360°) with a certain angle step, the two dimensional complex scattered amplitudes $w(q_x, q_y)$ (5) are merged into the three dimensional scattered amplitudes:

$$\text{Merge}[|A(q_x, q_y)|e^{-i*\varphi(q_x, q_y)}] = |A(\vec{q})|e^{-i*\varphi(\vec{q})} \quad (7)$$

The three dimensional *Fourier transform* of (7) gives the three dimensional **distribution of the electron density** in the real space:

$$\rho(\vec{r}) = \mathcal{F}_{3D}(|A(\vec{q})|e^{-i*\varphi(\vec{q})})$$

(8)

Consider the 2D **projections of the electron densities** obtained from the *curved* wave and *plane* wave fronts in the real space:

$$\tilde{p}(x, y) = \mathcal{F}_{2D}(|\tilde{A}(q_x, q_y)|e^{-i*\varphi(q_x, q_y)}) \rightarrow \text{Curved wave front}$$

(9)

$$p(x, y) = \mathcal{F}_{2D}(|A(q_x, q_y)|e^{-i*constant}) \rightarrow \text{Plain wave front,}$$

(10)

where the **projections of the electron densities** with a *plane* wave front have constant phase. And consider the Gaussian beam function:

$$g(x, y)$$

(11)

Then $\mathcal{F}_{2D}^{-1}\{\tilde{p}(x, y)\}$ can be written as the result of the convolution of $\mathcal{F}_{2D}^{-1}\{g(x, y)\}$ with $\mathcal{F}_{2D}^{-1}\{p(x, y)\}$:

$$\mathcal{F}_{2D}^{-1}\{\tilde{p}(x, y)\} = \mathcal{F}_{2D}^{-1}\{g(x, y)\} \otimes \mathcal{F}_{2D}^{-1}\{p(x, y)\}$$

(12)

The convolution takes place in the reciprocal space. Where:

$$|\mathcal{F}_{2D}^{-1}\{\tilde{p}(x, y)\}| = \tilde{A}(q_x, q_y)$$

(13)

is the distribution of the amplitudes on the detector in the two dimensional reciprocal space.

In this experiment we deal with the *curved* wave front, hence, it is reasonable to deconvolve $\mathcal{F}_{2D}^{-1}\{\tilde{p}(x, y)\}$ with $\mathcal{F}_{2D}^{-1}\{g(x, y)\}$ and approximate the distribution of the amplitudes on the detector in the two dimensional reciprocal space from the *plain* wave front :

$$A(q_x, q_y)_{deconv} = \left| \mathcal{F}_{2D}^{-1} \left\{ \frac{\tilde{p}(x, y)}{g(x, y)} \right\} \right|$$

(14)

And the corresponding phases from the *plane* wave front in the reciprocal space:

$$\varphi(q_x, q_y)_{deconv} = \text{angle}(\mathcal{F}_{2D}^{-1} \left\{ \frac{\tilde{p}(x, y)}{g(x, y)} \right\})$$

(15)

After performing the deconvolution for all perspectives (360°) with a certain angle step, the two dimensional complex scattered amplitudes (14) are merged into the three dimensional scattered amplitudes:

$$\text{Merge} \left[A_{deconv} e^{-i*\varphi(q_x, q_y)_{deconv}} \right] = |A_{deconv}(\vec{q})| e^{-i*\varphi(\vec{q})_{deconv}}$$

(16)

The three dimensional *Fourier transform* of (16) gives the three dimensional ***distribution of the electron density*** in the real space:

$$\rho(\vec{r}) = \mathcal{F}_{3D} \{ |A_{deconv}(\vec{q})| e^{-i*\varphi(\vec{q})_{deconv}} \}$$

(17)

3. Experimental problem

We have a Coherent *X-ray Diffraction Imaging (CXDI)* experiment with a monochromatic beam and a photon-counting pixel detector positioned in transmission geometry. The sample is a *colloidal crystal* placed downstream the focal plane.

It is essential for us to get the best possible resolution of the measured intensities on the detector from the sample. An important premise for the higher resolution is having a *plane* wave front. This can be achieved by placing the crystal in focus.

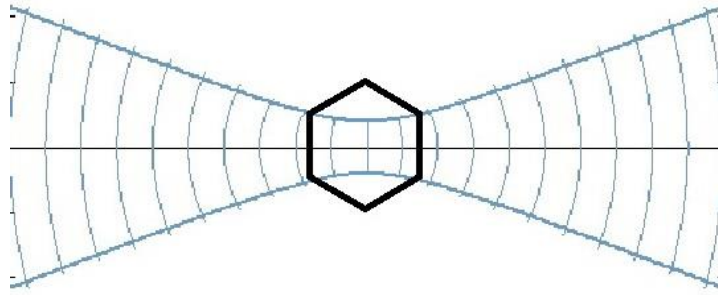


Figure 4: The sample is placed in the focus

In our experiment the size of the sample is larger than the size of the *beam* in the focus (Figure 5). The solution is to move the sample out of the focus.

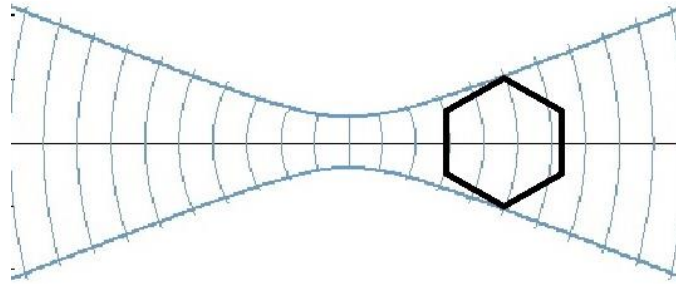


Figure 5: The sample is positioned out of the focus

Since, the sample is placed out of the focus we get *curved* wave front. The goal of this work is to investigate the influence of the *curved* wave front on the reconstruction quality and to improve it.

4. Simulation of the experiment

First, we used *Wolfram Mathematica* to construct the shape of the colloidal crystal with its predefined properties (colloidal spheres and sphere packing). The resulted *Wolfram Mathematica* simulation of the crystal was formatted to PDB (Protein Data Bank) file. Then the simulated colloidal crystal (in the PDB format) was processed by *Moltrans* – simulation program of the synchrotron beam propagating through the sample, written by Prof. Dr. Edgar Weckert. *Moltrans* returns the distribution of the intensities on the detector (diffraction image of the sample) with the corresponding phases of the wave in the far-field. All further computations with two dimensional *Moltrans* data have been performed in *Matlab*. Merging of the two dimensional *Matlab* results into three dimensional distributions of intensities, amplitudes, phases and electron densities has been done in C++ program.

5. Experiment setup

During the real experiment the sample was placed on the carbon fiber downstream the focal plane and was cooled with flow of nitrogen from the *Cryojet*. *Compound refractive lenses* (CRL) have been used.

Here are the parameters of the experiment:

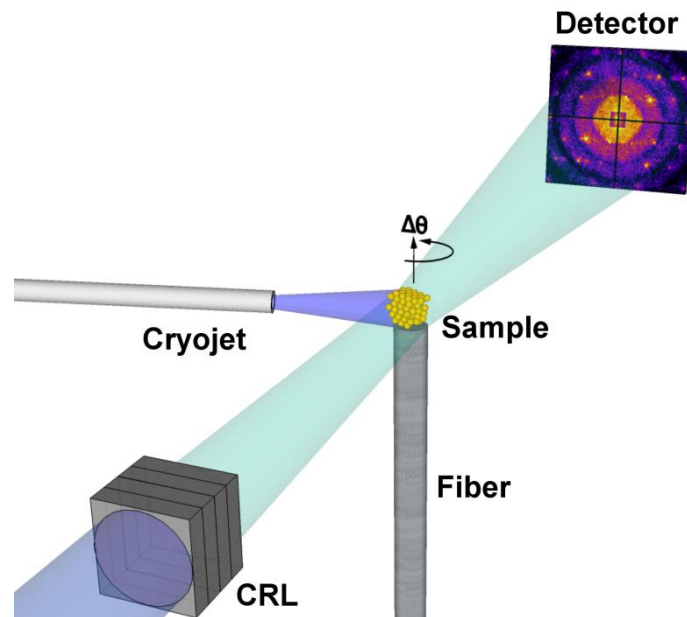


Figure 6: Experiment setup

The experiment has the following properties:

- *CXDI – Coherent X-ray Diffraction Imaging* experiment
- Monochromatic coherent X-ray beam, 7.9 keV
- Photon-counting pixel detector positioned in transmission geometry.
- Sample detector distance: 5.1 [m]
- Detector size: 28x28 [mm], 516x516[pixel], pixel size: 55 [μm]
- Gaussian beam size: $\sigma_z = 2.1$ [μm], $\sigma_y = 1.4$ [μm]
- Sample positioning: 11 [mm] downstream the focal plane (size of the focal spot 0.64x0.41 [μm^2])
- Wave front curvature: $R_z = 16.15$ [mm], $R_y = 15.4$ [mm]

The same parameters have been used for the simulation of the experiment.

6. Properties of the sample in the CXDI experiment

For the simulation of the crystal the icosahedron shape has been chosen. This shape corresponds to the generic one existing in the nature (so called geometrical primitives). On the other hand, it has faces and that means the diffraction image will contain *fringes*. It is valuable to have *fringes*, because they help to evaluate the quality of the diffraction image and its credibility. Here are the properties of the simulated sample (Figure 9) in the experiment:

- Sample: Colloidal crystal made of *polystyrene* spheres 220 nm in diameter. Grain size = 3 [um]
- Shape: Icosahedron (Figure 8)
- Structure: FCC – face centered cubic structure (layer sequence ABC). Figures 10 and 11.

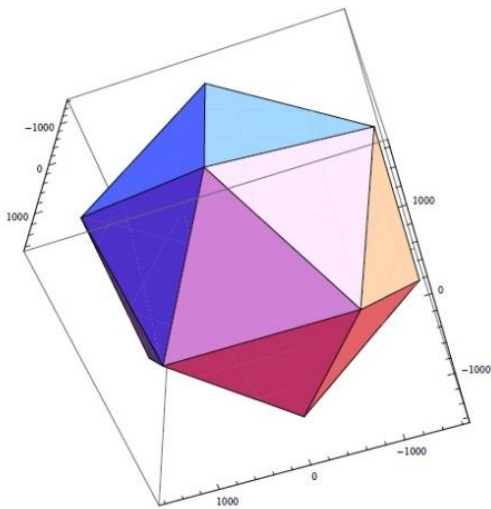


Figure 7: Icosahedron

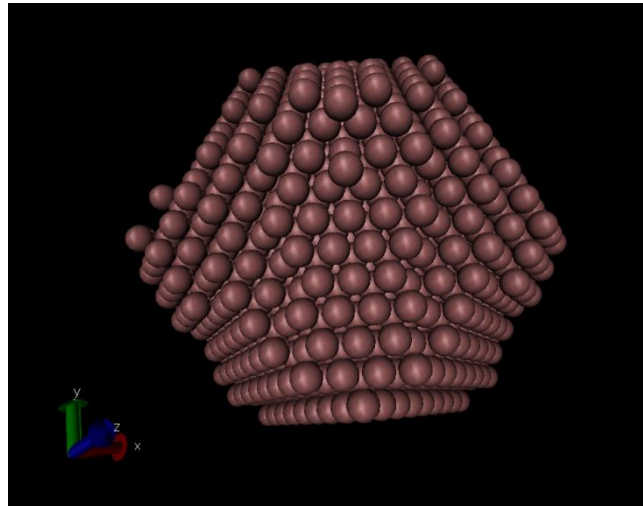


Figure 8: Simulation of the sample

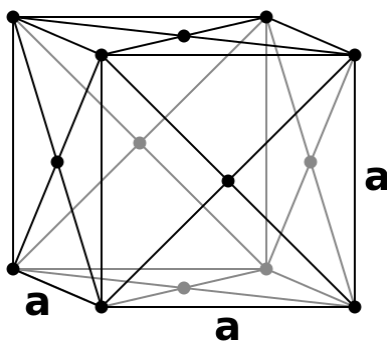


Figure 9: Face centric cubic structure (FCC)

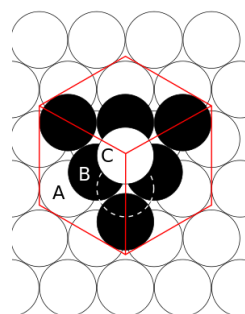


Figure 10: ABC sequence

7. Results

Diffraction images

In the presented two dimensional *diffraction images*, projection of the *electron density distribution* and *phases* in the real space, obtained from the simulation, the *Gaussian* beam hits icosahedron shaped colloidal crystal directly in one of the faces.

First, the diffraction images from the sample were obtained – with the *plane* (equation 5, figure 12), *curved* (equation 5, figure 13) wave fronts and then the result from the *deconvolution* (equations 14 and 15, figure 14).

The main goal of the *deconvolution* (equations 14 and 15) was to get rid of the blur on the diffraction images from the *curved* wave front. The blur caused lower resolution of the image. In order to compare the results and to draw conclusions *Bragg peaks*, *Streaks*, *Fringes* and *Form factor* of the colloidal particle are analyzed:

- **Bragg peaks** from the *curved* wave front are less clear compared to the *Bragg peaks* from the *plane* wave front. After the *deconvolution* Bragg peaks become rather clearer.
- **Form factor** is clearly recognizable from the *curved* and plain wave fronts, but practically vanishes after the *deconvolution*.
- **Streaks** after the *deconvolution* become clearer compared to the *plane* and wave fronts. As mentioned above, in this simulation the beam hits the icosahedron shaped colloidal crystal directly in one of the faces. The projection of the icosahedron in the beam direction on the plane is a hexagon. The direction of the *Streaks*, originating from the *Bragg peaks*, form hexagonal projection.
- **Fringes** after the *deconvolution* become clearer as well. All diffraction images are presented in the logarithmic scale.

Projection of the electron density distribution

The two dimensional projections of the *electron density distributions* from the *plane* (equation 10), *curved* (equation 9) wave front and deconvolution (equation 14) are presented on the figures 15, 16, 17. Here we can see only a slight improvement of the projection of the *electron density distribution* after the deconvolution.

Phases in the real space

When analyzing the phases $\varphi(q_x, q_y)$ on the figures 18, 19, 20 only values inside hexagon are of interest to us, the rest are artifacts.

Phases from the *curved* wave front that are near the hexagon sides are closer to zero (white region). The highest phase value is in the middle of the hexagon. Figure 18. *Plain* wave front has a constant phase and that is what we observe on the figure 19. The result of the deconvolution (equation 15) is a constant phase inside the hexagon, which is good result.

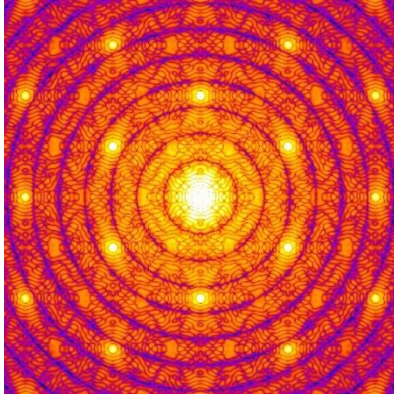


Figure 11: Plain wave front

$$A(q_x, q_y)$$

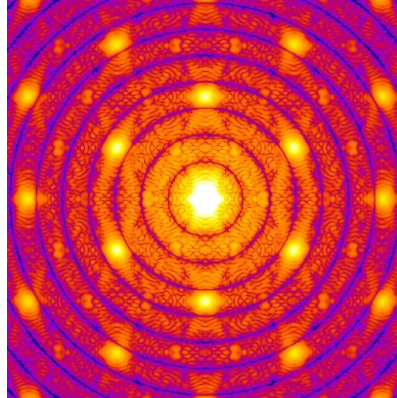


Figure 12: Curved wave front

$$\tilde{A}(q_x, q_y)$$

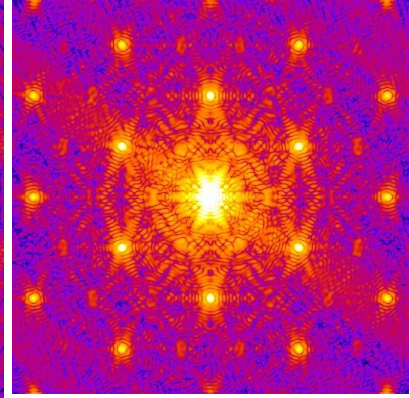


Figure 13: Deconvolution of the curved wave front with the Gaussian beam function

$$\left| FT\left(\frac{\tilde{p}(x, y)}{g(x, y)}\right) \right|$$

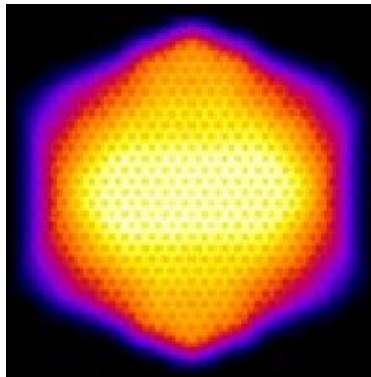


Figure 14: Plain wave front

$$p(x, y) = |A(q_x, q_y)|e^{-i*constant}$$

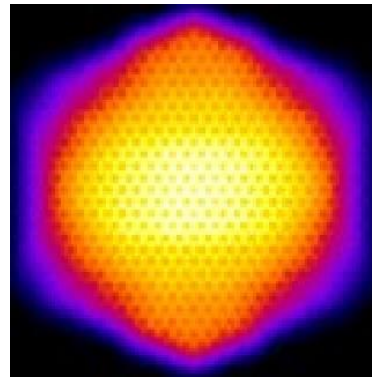


Figure 15: Curved wave front

$$\tilde{p}(x, y) = |\tilde{A}(q_x, q_y)|e^{-i*\varphi(q_x, q_y)}$$

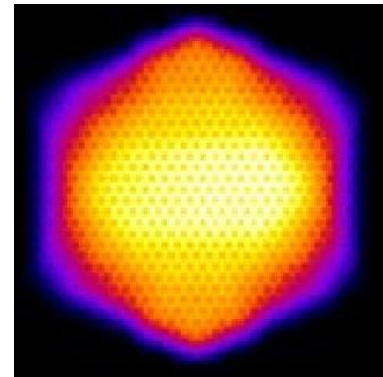


Figure 16: Deconvolution of the curved wave front with the Gaussian beam function

$$\frac{|\tilde{p}(x, y)|}{|g(x, y)|}$$

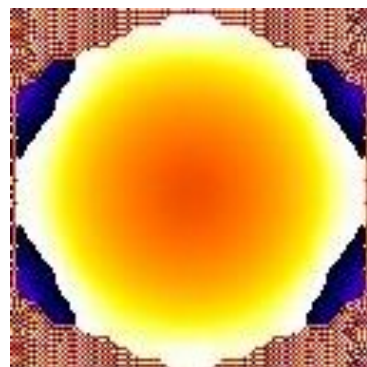


Figure 17: Plain wave front

$$angle(\mathcal{F}_{2D}\{\tilde{p}(x, y)\})$$



Figure 18: Curved wave front

$$angle(\mathcal{F}_{2D}\{p(x, y)\})$$

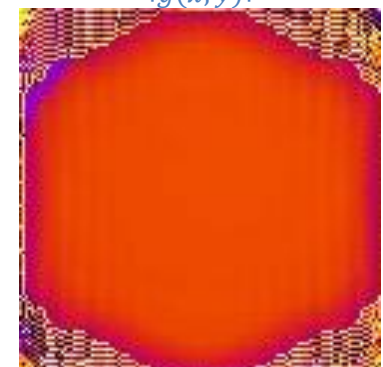


Figure 19: Deconvolution of the curved wave front with the Gaussian beam function

$$angle(\mathcal{F}_{2D}\left(\frac{\tilde{p}(x, y)}{g(x, y)}\right))$$

3D amplitudes distribution

After measuring the sample from all perspectives (360°) with a certain angle step, the two dimensional complex scattered amplitudes $w(q_x, q_y)$ (5) were merged into the three dimensional scattered amplitudes (equations 7 and 16; figures 21, 22 and 23).

3D electron density distribution

Figures 24, 25 and 26 depict the result of the three dimensional *Fourier transform* of the three dimensional scattered amplitudes, where the icosahedron shape of the colloidal crystal is recognizable. When comparing the *electron density distribution* from the *plain* wave front to the *curved* wave front, we can see that the *electron density distribution* from the *curved* wave front contains less colloidal particles. Deconvolution improves this matter significantly and more colloidal particles are present on the figure 26 than on the figure 24.

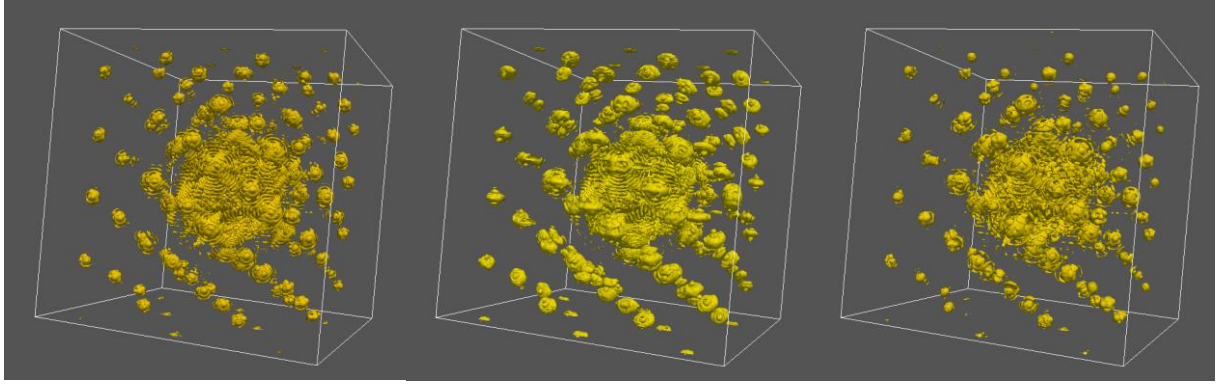


Figure 20: Plain wave front

Figure 21: Curved wave front

Figure 22: Deconvolution of the curved wave front with the Gaussian beam function

$$\text{Merge} \left[|A(q_x, q_y)| e^{-i*\varphi(q_x, q_y)} \right] \quad \text{Merge} \left[|\tilde{A}(q_x, q_y)| e^{-i*\varphi(q_x, q_y)} \right] \quad \text{Merge} \left[A_{deconv} e^{-i*\varphi(q_x, q_y)_{deco}} \right]$$

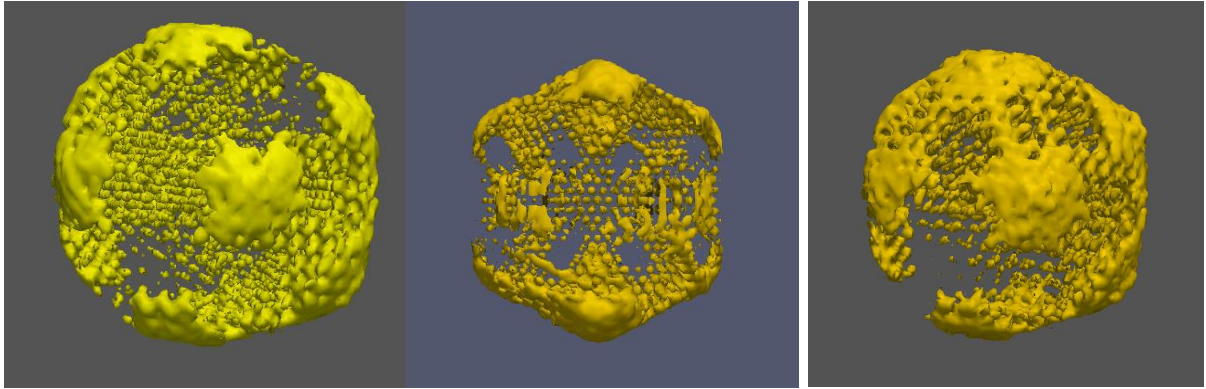


Figure 23: Plain wave front

Figure 24: Curved wave front

Figure 25: Deconvolution of the curved wave front with the Gaussian beam function

$$\rho(\vec{r}) = \mathcal{F}_{3D}\{|A(\vec{q})| e^{-i*\varphi(\vec{q})}\}$$

$$\rho(\vec{r}) = \mathcal{F}_{3D}\{|\tilde{A}(\vec{q})| e^{-i*\varphi(\vec{q})}\}$$

$$\rho(\vec{r}) = \mathcal{F}_{3D}\{A_{deconv}(\vec{q}) e^{-i*\varphi(\vec{q})_{deco}}\}$$

8. Conclusion

The *complex amplitude distribution*, *electron density distribution*, and *phases* (real space) in the approximation of the curved and plain wave fronts were obtained. Further, *deconvolution* of the *complex scattered amplitudes* with the *Gaussian beam function* (in reciprocal space) was performed.

Gaussian beam intensity distribution causes blur on the diffraction image in the reciprocal space and *curved phase* and lower resolution of the *electron density distribution* in the real space. The results indicate that blur of the diffraction image can be substantially minimized by the *deconvolution*, so the phase in the real space becomes constant and resolution of the *electron density distribution* is enhanced. The obtained results extend the existing technique of the coherent x-ray diffraction imaging.

9. Outlook

Next steps are to perform the complete phase retrieval algorithm first with the simulated data and then with the experiment data. Experimentally, the imitation of higher energies permits to increase resolution in the real space up to atomic range. The results are of interest for the Coherent X-ray Diffractive Imaging and for the study of the colloidal structures.

10. Acknowledgments

I would like to thank Prof. Dr. Edgar Weckert and Prof. Dr. Ivan Vartanyants for the mere opportunity of working in the X-Ray Crystallography Group at DESY and acquiring such a valuable knowledge. I want to thank Prof. Dr. Olaf Dössel from the Institute of Biomedical Engineering (IBT) at Karlsruhe Institute of Technology for giving me the chance to work at IBT and supporting my application for the DESY summer school. I am very thankful to Tobias Osterlein (IBT) for encouraging my first steps in science. I am very thankful to my supervisor Anatoly Shabalin from X-Ray Crystallography Group at DESY for his competent and friendly care and schooling. Many thanks to Ruslan Kurta and Dmirty Dzhigaev from X-Ray Crystallography Group at DESY for the expertise they share. I would also like to thank Sergey Lazarev, Max Rose for their help and my father Dr. Daniil Grigoriev for the rich advices during my work at DESY.

11. References

- [1] Jens Als-Nielsen, Elements of Modern X-ray Physics, Wiley, (2000)
- [2] J.-M. Meijer, A. Shabalin, R. Dronyak, O. M. Yefanov, R. P. Kurta, U. Lorenz, O. Gorobstov, D. Dzhigaev, J. Gulden, A. V. Zozulya, M. Sprung, I. A. Vartanyants and A. V. Petukhova, A. Singer, D. V. Byelov, Double hexagonal close-packed structure revealed in a single colloidal crystal grain by Bragg rod analysis, *Applied Crystallography*, **47**, 1, (2014)
- [3] A. Shabalin, E.A. Sulyanova, I. Besedin, O. Gorobstov, J.-M. Meijer, O. Yefanov, D. Dzhigaev, A. Zozulya Vartanyants, R.P. Kurta, M. Sprung, M. Krenkel, A. Petukhov and I.A., A.-L. Robisch, High resolution imaging of colloidal crystalline structures with a divergent X-ray beam